

Experimental measurements of the collapse of a two-dimensional granular gas under gravity

Reuben Son, John A. Perez, and Greg A. Voth

Department of Physics, Wesleyan University, Middletown, Connecticut 06459, USA

(Received 2 June 2008; published 2 October 2008)

We experimentally measure the decay of a quasi-two-dimensional granular gas under gravity. A granular gas is created by vibrofluidization, after which the energy input is halted, and the time-dependent statistical properties of the decaying gas are measured with video particle tracking. There are two distinct cooling stages separated by a high temperature settling shock. In the final stage, the temperature of a fluid packet decreases as a power law $T \propto (t_c - t)^\alpha$ just before the system collapses to a static state. The measured value of α ranges from 3.3 to 6.1 depending on the height, significantly higher than the exponent of 2 found in theoretical work on this problem [D. Volfson, B. Meerson, and L. S. Tsimring, *Phys. Rev. E* **73**, 61305 (2006)]. We also address the question of whether the collapse occurs simultaneously at different heights in the system.

DOI: [10.1103/PhysRevE.78.041302](https://doi.org/10.1103/PhysRevE.78.041302)

PACS number(s): 45.70.-n, 83.80.Fg, 47.57.Gc

I. INTRODUCTION

In a gravitational field, an undriven granular gas rapidly dissipates energy through inelastic collisions and returns to a static state. Although the processes of fluidization and collapse under gravity are important in granular materials processing, the decay of a granular gas under gravity has received surprisingly little attention [1]. One reason for the limited study of this problem is that under gravity the decay process is very inhomogeneous in both space and time. However, the inhomogeneity also makes this problem a valuable prototype since it provides a well controlled and experimentally realizable case of a granular material transitioning from a gas state to a static multiple-contact state.

There has been extensive work on the decay of granular gases without gravity [2,3]. Here the granular gas also develops density inhomogeneities due to the increased collision rate in dense clusters. For the model of hard spheres with constant coefficient of restitution, these gases exhibit inelastic collapse where an infinite number of collisions occur in a finite time. If the density inhomogeneity is suppressed, the system is known as a homogeneous cooling state. Here the temperature as a function of time, $T(t)$, decays according to Haff's law [4]: $T \propto t^{-2}$, which is a gradual decay rather than a collapse to a static state in a finite time.

When gravitational force is included, dense clusters are created at the lower boundary of a gas much more rapidly than clusters are created from fluctuations in the absence of gravity. As a result, inelastic collisions dissipate energy very quickly and after a finite time the material is at rest at the bottom of the chamber. We refer to this as gravitational-inelastic collapse [5] to highlight the central role that gravity plays in the process.

In a recent study, Volfson *et al.* [1] have analyzed a decaying granular gas under gravity using a hydrodynamic model and molecular dynamics simulations. They show that the hydrodynamic equations imply that the gravitational-inelastic collapse occurs simultaneously throughout the sample. Close to collapse they find that the granular temperature decays according to

$$T(y(m), t) = C(m)(t_c - t)^2, \quad (1)$$

where t is time, t_c is the collapse time beyond which the system is static, $y(m)$ is the position of Lagrangian mass

coordinate m , and $C(m)$ is a constant that depends on mass coordinate, but not time. They go on to argue that the total kinetic energy of the entire sample close to collapse should also decay as $(t_c - t)^2$. The vertical temperature profile $C(m)$, and the collapse time t_c depend on system parameters; however, the simultaneity of the collapse and the power law exponent of 2 are found to be general features of the hydrodynamic solutions and occur for a wide range of parameters, including parameters accessible to granular gases in the laboratory.

In this paper we study the decay and gravitational-inelastic collapse of an experimental quasi-two-dimensional (2D) granular gas. We wish to determine the phenomenology of particle velocity statistics during the decay, and in particular, to look for the scaling predicted by Volfson *et al.* [1] in an experimental system. The steady state of this system has been studied extensively [6–13]. A few studies have measured the time dependence of vertically vibrated granular gases under continuous vibration [14–16]. Here we create a granular gas by vertical vibration, and then halt the vibration so that the granular gas decays and undergoes a gravitational-inelastic collapse. We use high-speed video imaging to record particle trajectories during an ensemble of identical decay events. The moments of the particle velocity are measured as a function of space and time and we find that these fields allow the identification of regimes of the decay process. Finally, we study the late stages of the decay just before collapse to look for the power law predicted by Volfson *et al.* [1].

II. EXPERIMENTAL SETUP

Our granular gas is composed of $N=285$ borosilicate glass spheres of diameter $d=3.175$ mm. As shown in Fig. 1, the particles are confined to a quasi-two-dimensional space in a chamber with an aluminum frame and two glass viewing plates separated by $1.07d$. The cell is 92.3 mm \times 66.7 mm \times 3.4 mm, or equivalently, $29.07d \times 21.01d \times 1.07d$. In a hexagonally packed static state, the particles occupy 10 monolayers. The coefficients of normal restitution have been previously measured for glass spheres impacting a glass plate, $r=0.98$, and for glass spheres impacting an aluminum

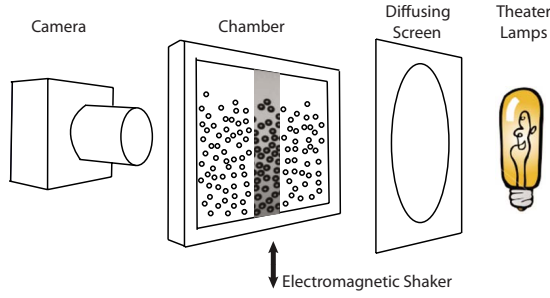


FIG. 1. (Color online) Schematic diagram of the apparatus. A high-speed video camera captures the motion of glass spheres confined between two glass plates. The chamber is backlit by a pair of theater lamps shining on an opal glass diffuser. Shown inside the chamber diagram is a raw image which closely represents the region of the chamber we image.

plate, $r=0.92$, with both showing a slight decrease with increasing velocity [17]. However, sphere-sphere impacts are expected to differ somewhat from the measured sphere-plate impacts. We choose to use the average of the measured values, $r=0.95$, when comparing with theoretical work. This is consistent with values used previously for glass spheres [13].

The chamber sits atop an electromagnetic shaker (LDS v450 from Ling Dynamic Systems). To create a granular gas, the chamber is vertically oscillated at frequency $f=100$ Hz with nondimensional acceleration $\Gamma=4\pi^2 f^2 A/g=35$ (oscillation amplitude, $A=870$ μm). After 50 oscillation cycles, the chamber motion is halted, and the granular gas decays to the bottom of the chamber. To halt the motion of the chamber quickly, we needed to determine the optimal force transient. If the system is modeled simply as a driven free mass, the force that would cause the mass to follow a Gaussian decay to the stationary equilibrium position would be

$$F \propto e^{-\omega^2 t^2/2}(\omega^2 t^2 - 1), \quad (2)$$

where the time $t=0$ is set at a position maxima of the sinusoidal oscillation. Rather than simply setting ω equal to the angular vibration frequency, we experimentally selected the value $\omega=1.4(2\pi f)$ because it minimized the time required for the chamber to come to rest. We were able to bring the chamber essentially to a halt within one drive cycle (0.01 s).

A high speed video camera (Basler A504k) is used to image the granular particle trajectories during the final two drive cycles and the entirety of the collapse to a static state. The chamber motion and imaging are synchronized by a computer running LABVIEW software. Signals generated in LABVIEW are processed through a digital-analog converter and are directed to the camera trigger and the shaker amplifier. Because the center of this system is nearly horizontally homogeneous, we focus on a vertical strip in the center of the cell, imaging the entire cell height ($21d$), but limiting the horizontal range of view to $3.65d$. This vertical strip can be imaged with 71×440 pixels, which allows a frame rate of 7000 Hz. This high frame rate allows us to resolve the granular temperature as far as possible into the decay. Because the system is computer controlled and accurately synchronized, it can produce many instances of the granular collapse,

which allows us to measure ensemble average statistics. The data presented in this paper consists of 1699 identically induced granular collapse events, each consisting of 2200 images.

From the image data, codes written in IDL extract positions of the centers of particles with an accuracy of $1/20$ of a pixel diameter, or equivalently, $d/390$ or 8.14 μm . The method used for finding the particle positions is to first use a standard particle finding algorithm to obtain approximate centers of the particles. Then we look along radial lines from the center of a particle to find the edge of the particle indicated by the sharp dark to bright transition. Averaging the positions of these transitions gives $1/20$ pixel position accuracy in both coordinates. Particles are then tracked by identifying the same particle in consecutive frames, and then velocities are determined by the displacement in one time step.

III. RESULTS

A. Substructure of a gravitational collapse

The trajectory data provides samples from the single-particle distribution function, $f(\vec{r}, \vec{v}, t)$ taken during an ensemble of collapse events. We visualize this data by calculating the moments of the velocity as a function of space and time as shown in Fig. 2. Our system is statistically one dimensional, so we show the vertical position on the vertical axis and time on the horizontal axis. The bin size is 4 pixels ($\approx \frac{d}{5}$) and 4 time steps (0.57 ms), which is sufficiently large to produce converged statistics, but small enough to resolve particle-scale structures and the rapid changes during the collapse.

Figure 2(a) shows the zeroth moment, or the density field. At late times, the density field shows periodic peaks reflecting the crystalline layering. These large variations occur because we use the particle centers to assign bins and the bin size is much smaller than a particle diameter. Figure 2(b) shows the mean vertical velocity $\langle v_y \rangle$. Figure 2(c) shows the vertical velocity variance $T_y(y, t) = \langle (v_y - \langle v_y \rangle)^2 \rangle$, often called the vertical granular temperature. Figure 2(d) shows the vertical velocity skewness defined as $S(y, t) = \langle (v_y - \langle v_y \rangle)^3 \rangle / T(y, t)^{3/2}$. The time origin is chosen to be the time when the shaking is halted. The height $y=0$ is the position of the lowest sphere after the collapse, which is $0.5d$ above the bottom of the chamber when it is at rest at $t \gg 0$.

In order to describe the diverse dynamics of the collapse, Fig. 3 shows the granular temperature field from Fig. 2(c) divided into regimes with similar dynamics. In regime A, the gas is characterized by shock waves that propagate upward from the bottom of the cell. As the shock waves travel upwards, the energy is dissipated by inelastic collisions and is also diffused since the initial shocks have a width less than a mean free path. Thus further up in the chamber, the amplitude of the shock waves decreases, and in regime B the time dependence of temperature essentially disappears. Here the gas is nearly homogeneously fluidized. When the driving force stops, regime B transitions into regime C. The particles cool quickly since they are no longer heated by the shock waves. The mean velocity [Fig. 2(b)] shows that in regime C the particles are accelerated downward by gravity. As the

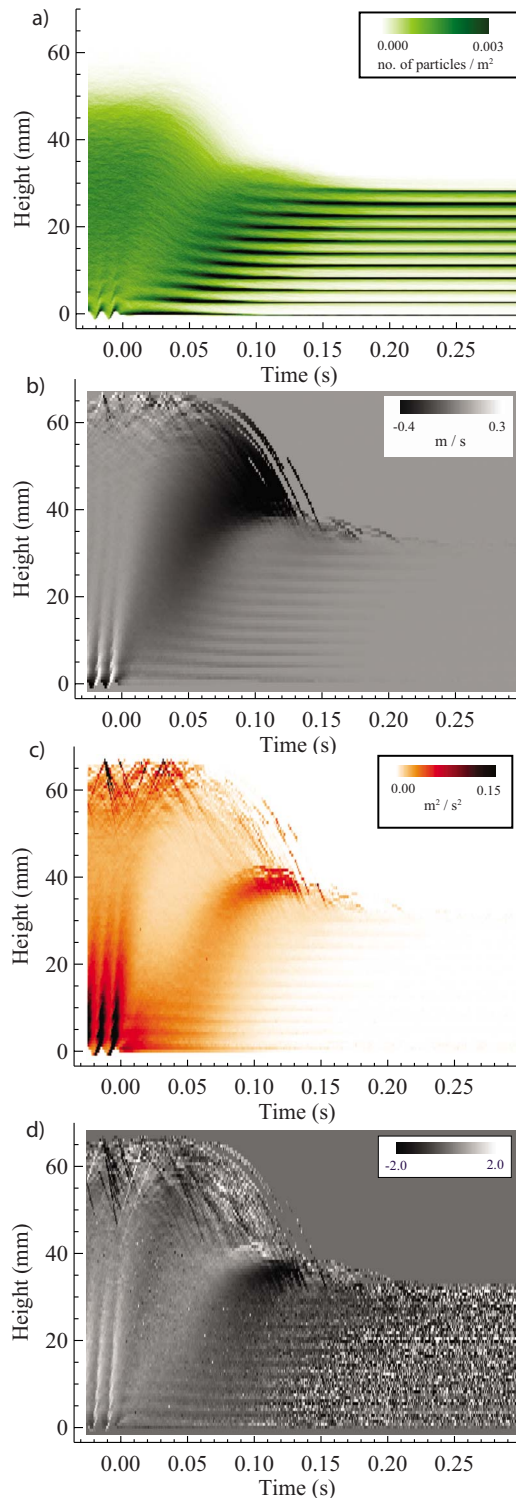


FIG. 2. (Color online) Moments of the vertical velocity as a function of height and time. (a) Density field. (b) Mean vertical velocity field. (c) Vertical velocity variance field. (d) Vertical velocity skewness field. The moments have been measured within each space-time bin and represented with a color map. For $t < 0$, the system is vertically vibrated, and at $t = 0$ the vibration is halted. The space axis represents the vertical position within the chamber, and $y = 0$ is defined as one particle radius above the bottom of the chamber at rest, which is the lowest position a particle center can occupy for $t \gg 0$.

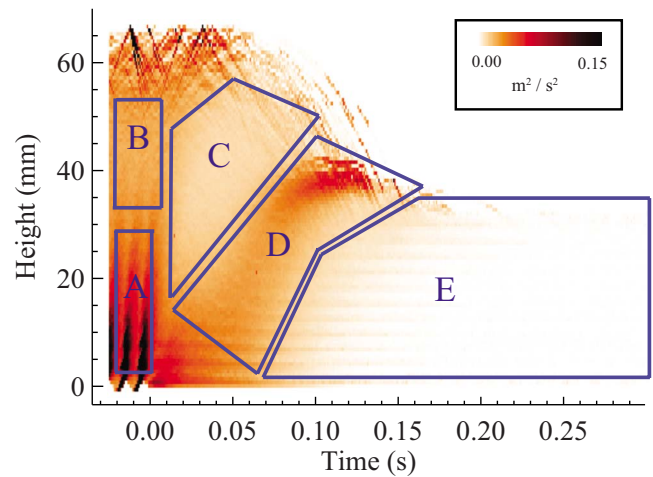


FIG. 3. (Color online) The temperature field of Fig. 2(c) with the regimes of the decay marked. Regime A is dominated by periodic heating from shock waves from the bottom wall. Regime B is a nearly time independent granular gas. Regime C is a freely cooling gas. Regime D is the settling shock. Regime E is the final cooling of a partially crystalline material until collapse.

cool falling gas meets the bottom of the chamber, a settling shock (regime D) forms where the energy in the mean velocity is converted to temperature. The density field [Fig. 2(a)] shows that in regime D, the low density falling gas collides with high density and partially crystallized material below. In regime E, the partially crystallized material loses energy rapidly because of the increasing rate of dissipative collisions, and approaches the static state.

We have also measured the fields for the moments of the horizontal velocity. Here the odd moments are nearly zero as expected because of horizontal reflection symmetry. The horizontal temperature field, $T_x(y, t)$, is qualitatively the same as the vertical component, but the shock waves of regime A and the settling shock of regime D are both slightly weaker. Weaker shock waves in the horizontal temperature make sense because gravity and the vertical vibration couple directly to the vertical velocity, while the energy only appears in the horizontal velocity after collisions.

Figure 2(d) shows the skewness of the vertical velocity. The first thing to note is that the skewness switches sign several times during the collapse and is consistently of order 1. Resolving the skewness at each space-time bin requires a huge number of velocity samples, and even with 1699 collapse events there remain large statistical fluctuations. Each shock wave has positive skewness at its leading edge. The beginning of regime C has negative skewness, while the leading edge of the settling shock returns to positive skewness. Finally, the beginning of regime E is characterized by large negative skewness as particles sometimes move rapidly into voids that open below them. In the later stages of regime E, the granular temperature is so small that the skewness is dominated by measurement error.

We have measured velocity statistics during decay and collapse for two other systems with a different number of particles in the chamber [17]. With either 5 or 15 monolayers of particles, the decay process is qualitatively similar. Al-

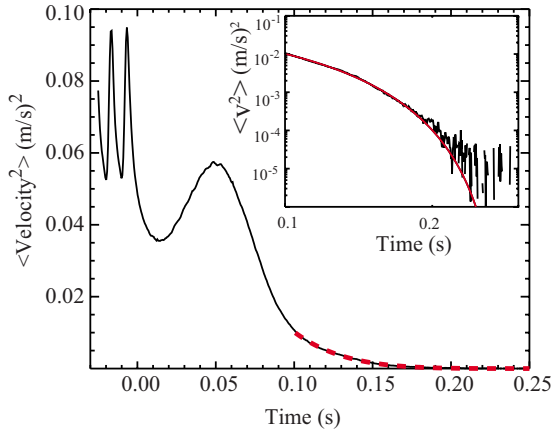


FIG. 4. (Color online) Second moment of the vertical velocity, $\langle v_y^2 \rangle$ for the entire system. The dashed line shows a power law fit with the exponent $\alpha=5.9$ for $0.1 \leq t \leq 0.28$. The inset is a log-log plot of the same energy decay and fit.

though we did not acquire nearly as much data on these two systems, it is clear that with more particles the decay occurs more quickly and the settling shock is better defined.

A few details in Fig. 2 are worth studying more carefully. In the density field [Fig. 2(a)], the shock waves in regime A are just visible, and they show substructure on the scale of a particle (3.175 mm). This substructure is also barely visible in the other fields in Fig. 2. An investigation of the substructure in these shocks is in preparation [18]. Also note in the mean velocity and velocity variance plots that there are ballistic particles that appear to the upper right of regime C. These particles continue to impact the top of the dense material all the way until $t=0.15$ s and as a result there is a very high temperature region that is sustained near the top of the dense material between $t=0.10$ s and $t=0.15$ s.

B. Power laws in late stages of collapse

These collapse regimes detail the general phenomenology of a granular collapse event. In particular, we note that the collapse of the gas involves two cooling stages, separated by a settling shock. In the latter cooling stage, Volfson *et al.* [1] have proposed that the total translational kinetic energy is dissipated as a power law: $E(t) \sim (t_c - t)^2$ as $t \rightarrow t_c$.

Figure 4 shows the second moment of the vertical velocity which is proportional to the vertical kinetic energy. The constant contribution from measurement error was determined by the offset well after collapse and has been subtracted from this and subsequent plots. Also shown is a non-linear fit to the late stage of decay using the functional form $E=C(t_c-t)^\alpha$, where t_c , α , and C are free parameters. In the late stages, the energy appears to decay as a power law, but the exponent in the fit is $\alpha=5.9$ rather than 2 as found in [1].

A more complete picture of the late stages of collapse emerges by following the decay of the temperature of a single fluid packet. This is accomplished by separating the system by the Lagrangian mass coordinate, defined as the fraction of the particles with height less than y ,

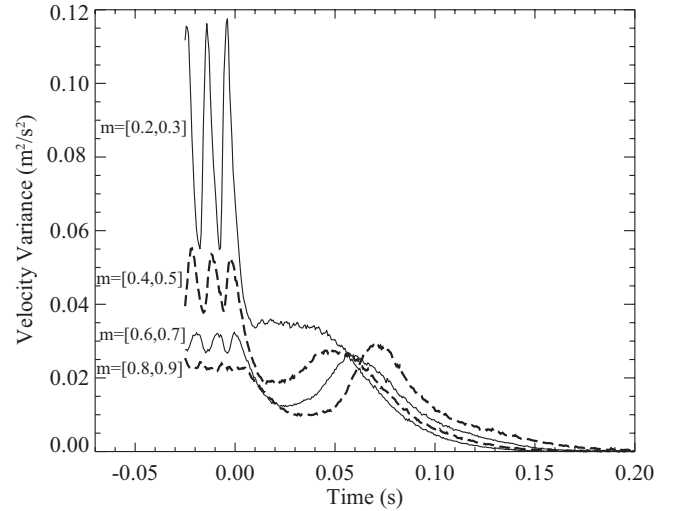


FIG. 5. Vertical velocity variance (vertical temperature) as a function of time for mass coordinate windows [0.2–0.3], [0.4–0.5], [0.6–0.7], and [0.8–0.9].

$$m(y,t) = \frac{\int_0^y n(y',t) dy'}{\int_0^{y_{\max}} n(y',t) dy'}, \quad (3)$$

where $n(y,t)$ is the number density, y_{\max} is the top of the chamber, and $0 \leq m \leq 1$. The limitations of using Eulerian coordinates is evident when an attempt is made to trace $T(y,t)$ across a fixed height y in Fig. 2(c). At some heights, the system has no particles after a short time and the temperature is undefined.

One of the most striking findings in [1] is that the temperature of a fluid packet decays as

$$T(y(m),t) = C_m(t_c - t)^2, \quad (4)$$

for $t \rightarrow t_c$, where $y(m)$ is the position of the fluid packet with mass coordinate m , and C_m depends only on mass coordinate. This implies that the temperature decay has the same power law exponent and the collapse time t_c is simultaneous at all heights. Next, we will evaluate the degree to which our data supports Eq. (4).

In Fig. 5, the vertical velocity variance $T_y(y(m),t)$ is plotted as a function of time for four different mass coordinate ranges that each span 10% of the sample. For $t < 0$, the higher mass coordinates experience smaller oscillations in temperature because the shock waves dissipate as they propagate upward. For $t > 0$, higher mass coordinates experience higher temperatures in the settling shock, and maintain higher temperature throughout the decay. These facts can be understood as reflecting the larger change in gravitational potential energy at large m and the lower gravitational pressure head which allows lower density at similar temperatures and hence slower inelastic energy loss. Qualitatively, this agrees with the temperature profiles observed in [1], where C_m was found to be larger at higher m .

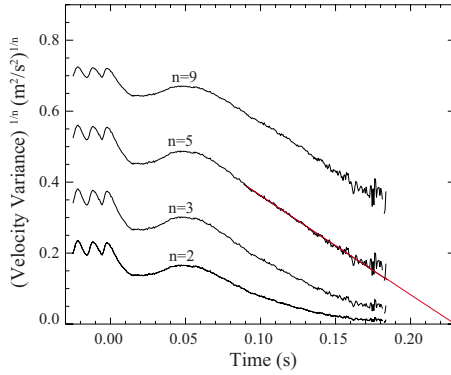


FIG. 6. (Color online) Vertical temperature $T_y(m, t)$ for mass coordinate window $m=[0.4-0.5]$, taken to several fractional powers: $n=2, 3, 5$, and 9 . The greatest linearity is observed for $n=5$. A nonlinear fit of functional form $T=C(t_c-t)^n$ with the best fit $n=5.2$ has been plotted on top of $T(y(m), t)^{1/5}$ to demonstrate the strength of the fit. All of the plots depicted have been cut off at $t \approx 0.18$ s due to the fact that raising $T(y(m), t)$ to a fractional power greatly amplifies the noise in the data.

To evaluate the existence of a power law at late times during the collapse, Fig. 6 shows $T_y(m, t)$, for $m=[0.4-0.5]$, raised to several different fractional powers. The lowest curve is raised to the $1/2$ power, and shows clear upward curvature rather than the straight line predicted by Eq. (4). However, the plot of $T^{1/5}$ is nearly linear, indicating that the decay is consistent with a power law, but with an exponent of 5. The plot of $T^{1/9}$ shows a slight downward curvature, restricting the plausibility of a power law to the vicinity of $n=5$. Note that with the limited scaling range it is not possible to definitively determine whether or not the decay is a power law. However, the data unambiguously shows that the data is consistent with a power law with $\alpha=5$ but not $\alpha=2$.

To determine how the final decay power law changes at different mass coordinates, we performed nonlinear fits of the function $T=C(t_c-t)^\alpha$ to the temperature measurements for each mass coordinate range. The best fit values of α and t_c are shown in Table I for both the vertical and horizontal temperature. An immediate conclusion is that the exponents for all mass coordinates are significantly greater than 2. The lower mass coordinates have slightly larger exponents ranging up to 6.1, and the higher mass coordinates have slightly smaller exponents with a minimum of 3.3. The collapse time shows a slight trend towards later collapse times at the top of the sample. The fit range was chosen iteratively to span the range from 14 ms before the collapse to the time when the temperature was smaller than 10^{-4} (m/s)^2 where measurement error dominates. We tried many different fit ranges and found that reasonable choices changed the power law exponents by roughly $\pm 10\%$. We then determined the uncertainty in $t_{c(y)}$ by fixing α_y to $\pm 10\%$ of the best fit and finding the change in best fit collapse time.

Figure 7 shows the position of the settling shock and the collapse time $t_{c(y)}$ superimposed on the vertical temperature field. The position of the settling shock was determined by finding the local maxima after $t=0$ in the temperature at each mass coordinate (see Fig. 5). An interesting observation is

TABLE I. Power law exponents and collapse time for ten different mass coordinates from fits to the temperature decay of the horizontal (x) and vertical (y) velocities. Errors for the y collapse time were estimated by varying $\alpha_y \pm 10\%$ and measuring $t_{c(y)}$ for the resulting best fit. These should be considered rough estimates.

Mass coordinates	Power law exponent		Collapse time	
	α_x	α_y	$t_{c(x)}$ (ms)	$t_{c(y)}$ (ms)
m				
[0.9-1.0]	3.3	4.1	264	275 ± 9
[0.8-0.9]	3.6	4.1	258	266 ± 8
[0.7-0.8]	3.6	3.9	228	242 ± 10
[0.6-0.7]	4.3	4.3	229	234 ± 18
[0.5-0.6]	5.1	4.5	236	229 ± 15
[0.4-0.5]	5.3	5.2	221	232 ± 15
[0.3-0.4]	5.3	5.2	222	213 ± 11
[0.2-0.3]	5.6	6.1	218	225 ± 13
[0.1-0.2]	5.9	5.8	226	215 ± 11
[0.0-0.1]	5.1	5.3	226	209 ± 7

that the local maxima is shortly after $t=0$ for the first three mass coordinate ranges, but is significantly later for mass coordinates above $m=0.4$. We interpret this as a change in the dynamics of the settling shock as the density distribution shifts from the initial shock fluidized state (regime A) to the free-fall state (regime C). The collapse time t_c is nearly simultaneous at the lower mass coordinates, in agreement with the results of [1]. The top two mass coordinates are clearly later than the rest. There is a slight trend of the final collapse occurring later for higher mass coordinates, following the trend of the settling shock.

C. Bias due to limited frame rate

The frame rate at which the image data is taken is not a physical parameter of the granular gas, but it is a potentially significant parameter in our data. At too low a frame rate, densely packed particles may collide between frames and the camera records a displacement between frames that is smaller than the actual displacement [19]. In order to mea-

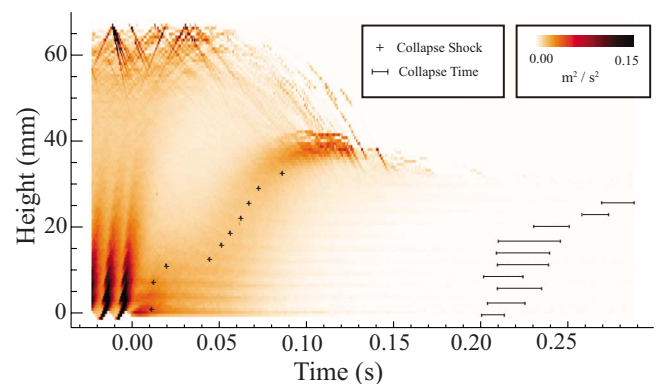


FIG. 7. (Color online) The settling shock peak and the collapse time $t_{c(y)}$ for all ten mass coordinate windows plotted on top of the vertical temperature field.

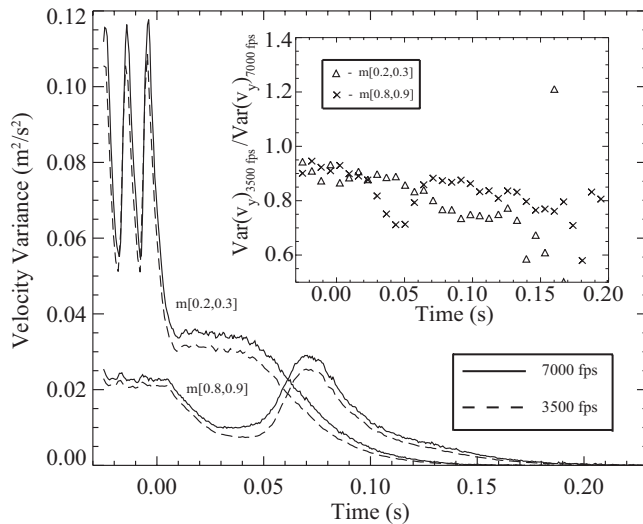


FIG. 8. The effects of reduced frame rate on vertical temperature measurements. Solid lines are for 7000 Hz frame rate and dashed lines are for 3500 Hz. The upper pair of curves are for mass coordinate $m=[0.2,0.3]$, and the lower pair are for $m=[0.8,0.9]$. Inset: Ratio of the vertical velocity variance for half frame rate to the value for full frame rate.

sure the effects of frame rate on our data, we ignored every other frame as if the data was taken at 3500 Hz. In Fig. 8 we compare two different mass coordinate ranges and observe that $T_{3500}(m, t) < T_{7000}(m, t)$ for all t . In the range of time in which we fit power laws to the temperature decay data, T_{3500} is approximately 80% of T_{7000} . The difference in power law exponents of the best fits to the temperature decay shows negligible dependence on the frame rate. For mass coordinate $m=[0.2,0.3]$, α from data sampled at 7000 Hz is 6% larger than α from the 3500 Hz data. For mass coordinate $m=[0.8,0.9]$, α was unchanged. Frame rates much larger than 7000 Hz are needed to fully resolve the later stages just before collapse, but the deviation from the exponent $\alpha=2$ predicted in [1] does not seem to be caused by limited frame rate.

D. Discussion

We have observed that the final stage of the decay of a granular gas under gravity shows a power law decay of the temperature, $T(y(m), t) \propto (t_c - t)^\alpha$ as found in Volfson [1]. However, we measure the power law exponent to be in the range $3.3 < \alpha < 6.1$ rather than $\alpha=2$ that they predict. The collapse time t_c is found to be simultaneous within measurement error for much of the system in agreement with Ref. [1], but there is a trend towards later collapse near the top of the chamber. Here we discuss factors that may be responsible for the differences between our experiment and Volfson *et al.* [1].

Although the parameters in our experiment are somewhat different than those used in the MD simulations in Ref. [1], this does not appear to be the cause of the discrepancy. Volfson *et al.* [1] use the nondimensional parameters $\epsilon = (\sqrt{\pi} N_y)^{-1}$ and $\Lambda^2 = \frac{1-r^2}{4\epsilon^2}$, where r is the coefficient of resti-

tution and $N_y = Nd/L_x$ is the number of static layers (here N is the total number of particles, d is the particle diameter, and L_x is the horizontal size of the chamber). In our experiment, $\epsilon = 5.7 \times 10^{-2}$ and $\Lambda \approx 0.43$, for a coefficient of restitution of $r=0.95$. For comparison, $\epsilon=10^{-2}$ and $\Lambda=5$ with $r=0.995$ are used in the MD simulations in Ref. [1]. However, their analysis of the hydrodynamic equations yields the prediction $T(y(m), t) \propto (t_c - t)^2$ for both $\Lambda \ll 1$ and $\Lambda \gg 1$ with the implication that this scaling is a general feature of gravitational-inelastic collapse.

The experiment differs from the 2D hard sphere system analyzed in [1] in several ways. The interactions between our glass spheres are significantly more complicated than the frictionless hard spheres used in Ref. [1]. The most significant difference is probably the frictional interactions, but the finite elastic modulus may matter as well. Our experiment has gaps of $1.07d$ between the glass confining plates, so there is some motion in the third dimension. The glass plates also introduce an additional source of friction in the system [11]. In the late stages of the decay, the system partially crystallizes, but presumably this also occurs in the monodisperse 2D molecular dynamics simulations.

We think that the frictional interactions are likely the most important of these effects. Friction with the confining walls of the quasi-2D chamber provides an additional frictional contact, but we suspect that particle-particle friction is sufficient to produce the deviations. Future experiments could test this by changing the frictional interactions between particles, either by adding a lubricant such as graphite or by using particles of different materials. It would also be interesting to use molecular dynamics simulations to study the effects of friction on gravitational-inelastic collapse to determine whether the power law exponent near collapse depends on friction.

IV. CONCLUSIONS

We have performed experimental measurements of particle trajectories in a time-dependent granular gas decaying under gravity. By repeated acquisition of a large number of identical decay events, we obtained measurements of the moments of the velocity distribution with good resolution in space and time. The measured fields of density, mean velocity, temperature, and skewness show several distinct regimes that the gas progresses through before collapse. After vibrational energy input is halted, the gas cools rapidly and falls toward the bottom of the chamber. As the falling material encounters the bottom boundary, a settling shock forms that propagates upward through the sample. After the settling shock, the gas enters a second and final cooling stage that ends with collapse to a static state.

Measurements of the temperature of a fluid packet just before collapse show that the temperature decays as a power law, $T(y(m), T) = (t_c - t)^\alpha$, but that the exponent is $3.3 < \alpha < 6.1$, significantly greater than the value of $\alpha=2$ found in [1]. The collapse time t_c slightly increases toward the top of the sample, but the differences are smaller than the measurement error through much of the sample.

The process of the decay and collapse of a fluidized granular material under gravity is fundamental to under-

standing many kinds of granular flows. The system studied in this paper provides a simple and well controlled experimental realization of the decay and collapse process. Experiment and theory agree on the qualitative features during decay, and on the existence of a power law approach to collapse. However, the discrepancy in the power law exponent suggests that more work is needed to develop a quantitative understanding of gravitational-inelastic collapse.

ACKNOWLEDGMENTS

This work was supported by Wesleyan University, the Alfred P. Sloan Foundation, and NSF Grant No. DMR-0547712. We thank Mark Shattuck for many insights and Takanori Nagatomo and Kin Yan Chew for their work developing the experiment.

-
- [1] D. Volfson, B. Meerson, and L. S. Tsimring, *Phys. Rev. E* **73**, 061305 (2006).
- [2] I. Goldhirsch, *Annu. Rev. Fluid Mech.* **35**, 267 (2003).
- [3] N. Brilliantov and T. Poschel, *Kinetic Theory of Granular Gases* (Oxford University Press, Oxford, 2004).
- [4] P. K. Haff, *J. Fluid Mech.* **134**, 401 (1983).
- [5] D. Ertas and T. C. Halsey, *Europhys. Lett.* **60**, 931 (2002).
- [6] S. Warr, J. M. Huntley, and G. T. H. Jacques, *Phys. Rev. E* **52**, 5583 (1995).
- [7] S. McNamara and S. Luding, *Phys. Rev. E* **58**, 813 (1998).
- [8] F. Rouyer and N. Menon, *Phys. Rev. Lett.* **85**, 3676 (2000).
- [9] K. Feitosa and N. Menon, *Phys. Rev. Lett.* **88**, 198301 (2002).
- [10] B. Meerson, T. Poschel, and Y. Bromberg, *Phys. Rev. Lett.* **91**, 024301 (2003).
- [11] J. S. van Zon, J. Kreft, D. I. Goldman, D. Miracle, J. B. Swift, and H. L. Swinney, *Phys. Rev. E* **70**, 040301(R) (2004).
- [12] Sung Joon Moon, J. B. Swift, and H. L. Swinney, *Phys. Rev. E* **69**, 011301 (2004).
- [13] P. Eshuis, K. van der Weele, D. van der Meer, R. Bos, and D. Lohse, *Phys. Fluids* **19**, 123301 (2007).
- [14] J. Bougie, Sung Joon Moon, J. B. Swift, and H. L. Swinney, *Phys. Rev. E* **66**, 051301 (2002).
- [15] X. Y. Yang, C. Huan, D. Candela, R. W. Mair, and R. L. Walsworth, *Phys. Rev. Lett.* **88**, 044301 (2002).
- [16] K. Huang, G. Miao, P. Zhang, Y. Yun, and R. Wei, *Phys. Rev. E* **73**, 041302 (2006).
- [17] J. Perez, Ph.D. thesis, Wesleyan University, 2006 (unpublished).
- [18] J. Perez, S. Kachuck, and G. Voth, *Phys. Rev. E* (to be published).
- [19] H. T. Xu, A. P. Reeves, and M. Y. Louge, *Rev. Sci. Instrum.* **75**, 811 (2004).